POLITECNICO DI TORINO
Repository ISTITUZIONALE

A Detailed Analysis and Guidelines for the Induction Motor Flux-Decay Test

Original
A Detailed Analysis and Guidelines for the Induction Motor Flux-Decay Test / Armando, E., Boglietti, A., Mandrile, F., Carpaneto, E., Rubino, S.. - In: IEEE TRANSACTIONS ON INDUSTRY APPLICATIONS. - ISSN 0093-9994. - (2024), pp. 1-9. [10.1109/TIA.2023.3297983]

Availability:
This version is available at: 11583/2980665 since: 2023-07-25T11:47:17Z

Publisher:
IEEE

Published
DOI:10.1109/TIA.2023.3297983

Terms of use:

This article is made available under terms and conditions as specified in the corresponding bibliographic description in the repository

Publisher copyright
IEEE postprint/Author's Accepted Manuscript

©2024 IEEE. Personal use of this material is permitted. Permission from IEEE must be obtained for all other uses, in any current or future media, including reprinting/republishing this material for advertising or promotional purposes, creating new collecting works, for resale or lists, or reuse of any copyrighted component of this work in other works.

(Article begins on next page)

18 November 2026

A Detailed Analysis and Guidelines for the Induction Motor Flux-Decay Test

Eric Armando, *Senior Member, IEEE*, Aldo Boglietti, *Fellow, IEEE*, Fabio Mandrile, *Member, IEEE*, Enrico Carpaneto, *Member, IEEE*, and Sandro Rubino, *Member, IEEE*

***Abstract*--Ac motor drives are becoming increasingly popular in the field of industrial processes and transportation electrification. Currently, many industrial applications are based on induction machines supplied by inverters and controlled with field-oriented control techniques. Such techniques require the knowledge of the machine parameters to ensure the correctness of the torque control both in dynamic and steady-state conditions. In particular, an accurate determination of the induction motor rotor time constant is crucial. Therefore, this paper analyses in detail the physical phenomena involved during the flux-decay test used for the rotor time constant determination. The reported analysis has been performed on a 15 kW induction motor. The transient of the machine's back-electromotive force (back-emf) has been critically analyzed during its evolution, finding a link between its evolution in time and the magnetic phenomena that occur both in the stator and the rotor. In particular, the effects due to the lamination saturation, the stator and rotor leakage inductances, and the stator iron losses have been associated with the transient evolution of the machine's back-emf.**

***Index Terms*--Induction motor, rotor time constant, field-oriented control, flux-decay test, no-load test.**

NOMENCLATURE

$v_{123}^s = [v_1^s \ v_2^s \ v_3^s]$	Stator voltages in phase coordinates (V);
$v_{\alpha\beta}^s = [v_\alpha^s \ v_\beta^s]$	Stationary stator voltages (V);
$i_{\alpha\beta}^s = [i_\alpha^s \ i_\beta^s]$	Stationary stator currents (A);
$i_{\alpha\beta}^r = [i_\alpha^r \ i_\beta^r]$	Stationary rotor currents (A);
$e_{\alpha\beta}^s = [e_\alpha^s \ e_\beta^s]$	Stationary stator back-emf (V);
e^s	Stator back-emf amplitude (V);
f_s	Stator frequency (Hz);
f_r	Rotor frequency (Hz);
s	Motor slip;
$[T_C]$	Clarke transformation;
R_s	Stator resistance (Ω);
R_r	Rotor resistance (Ω);
L_s	Stator inductance (H);
L_r	Rotor inductance (H);
L_m	Magnetizing inductance (H);
L_{ls}	Stator leakage inductance (H);
L_{lr}	Rotor leakage inductance (H);
ω_r	Rotor electric speed (rad/s);
p	Motor pole pairs;
τ_r	Rotor time constant (s);
$R_{r,eq}$	Equivalent rotor resistance (Ω);
$\tau_{r,eq}$	Equivalent rotor time constant (s);
R_{ir}	Equivalent rotor resistance due to the stator iron losses (Ω);
I_0^r	Initial rotor current vector amplitude (A);
ϑ_0^r	Initial rotor current vector position (rad);
Λ_0^r	Initial rotor flux linkage (Vs);
ϑ_0^s	Initial stator voltage vector position (rad);
Y, X_0, τ	Variables for fitting the exponential profiles.

I. INTRODUCTION

MODERN ac motor drives are nowadays becoming ever more popular in several industrial sectors thanks to their high performance, reliability, and ruggedness. Many of these applications rely on induction machines supplied by inverters. The state-of-the-art about torque control of such machines is the well-known field-oriented control (FOC), which regulates the machine's torque by directly controlling the machine's (*dq*) currents [1]. To do so, the FOC scheme requires the rotor flux angle to correctly orient the control reference system to the physical axes of the machine.

In the literature and industrial practice, two FOC algorithms are mainly available. The first solution is the direct field-oriented control (DFOC), which estimates the rotor flux vector by implementing either full-order or reduced-order observer starting from measured electrical (stator currents) and mechanical quantities (rotor speed) [2]. The second option is the indirect field-oriented control (IFOC), which indirectly calculates the rotor flux orientation using only the measured rotor speed and the estimated slip frequency from the reference (*dq*) stator currents. The IFOC allows a more straightforward sensing technique than the DFOC since it does not rely on observers and current feedback to obtain the rotor flux orientation. For this reason, the IFOC is the most commonly implemented solution in induction motor drives [2].

In general, FOC-based control schemes require an accurate estimation of the rotor time constant to accomplish proper torque regulation [3]. Therefore, an estimation error of the rotor time constant leads to the derating of the control performance [4]. The technical literature provides several approaches to estimating the rotor time constant of induction machines.
Some methods are based on dedicated machine supply schemes (dc and ac) with transient tests and post-process analyses to evaluate the rotor time constant [5], [6]. Other methods are

The authors are with Dipartimento Energia "G. Ferraris", Politecnico di Torino, 10129 Turin, Italy (eric.armando@polito.it, aldo.boglietti@polito.it, fabio.mandrile@polito.it, enrico.carpaneto@polito.it, and sandro.rubino@polito.it).

executed while the machine is operated in closed-loop speed control, using dedicated control algorithms [7], Kalman estimators [8], [9], neural networks and fuzzy logic [10], [11], and model reference adaptive systems [12], [13], all involving a significant computational effort.

This paper starts from the preliminary results presented in [14], [15], and it considers a straightforward experimental method based on the flux-decay test at no-load conditions. In this test, the machine is initially supplied with a certain stator voltage level to magnetize the rotor. Then, the machine supply is suddenly turned off, and the stator back-emf is measured. Finally, the rotor time constant is evaluated by analyzing the back-emf's decay. Despite being a straightforward method, identifying the time constant from the back-emf decay transient can present some challenges related to the design of the rotor of the induction machine.

Therefore, the contribution of this paper is the detailed analysis of the physical phenomena involved in the flux-decay transient. In this analysis, the most significant phenomena involved in the flux-decay transients are analyzed for the first time and linked to the inner electromagnetic quantities of the induction machine. Moreover, several guidelines are provided to identify the correct time constant of the machine, which can then be employed for torque control in FOC algorithms, as demonstrated in [16].

The paper is organized as follows. In Section II, the flux-decay test methodology is briefly summarized. Then, in Section III, the reference flux-decay waveforms considered in this paper are presented, as well as the fitting procedure to identify the rotor time constant. The core contributions of this paper are presented in Section IV, reporting a detailed analysis of the electromagnetic phenomena involved in the flux-decay test and the guidelines for elaborating the flux-decay test results. Finally, the conclusions are drawn in Section V.

II. Description of the Flux-Decay Test

In the flux-decay test, the induction motor is initially supplied with the rated stator voltage and frequency and operated in no-load torque conditions. Then, the stator winding is disconnected from the supply using an electromechanical switch. During the test, it is only necessary to measure the stator voltages and record their evolution after the disconnection process. The voltage measurements can be performed using a calibrated data sample recorder and an experimental setup, as shown in Fig. 1. It must be pointed out that the variable three-phase generator can be either a sinusoidal source or the target inverter for the electric drive.

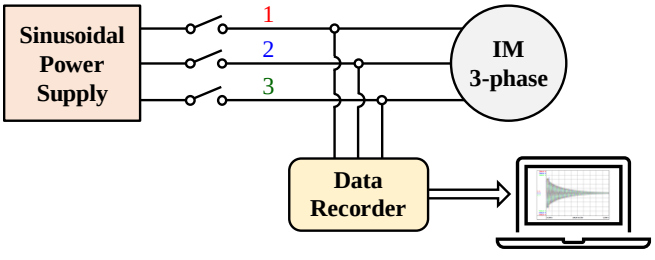


Fig. 1. Experimental setup for performing the flux decay test.

The flux-decay can be explained using the induction motor dynamic equations and by describing the electromagnetic phenomena involved in the machine. In detail, the evolution of the rotor currents during the flux-decay test can be obtained starting from the induction motor equations in the stationary (αβ) reference frame. Before the stator supply is disconnected, the machine's equations can be written as [17]:

$$\begin{cases} v_\alpha^s = R_s \cdot i_\alpha^s + L_s \cdot \dfrac{di_\alpha^s}{dt} + L_m \cdot \dfrac{di_\alpha^r}{dt} \\ v_\beta^s = R_s \cdot i_\beta^s + L_s \cdot \dfrac{di_\beta^s}{dt} + L_m \cdot \dfrac{di_\beta^r}{dt} \\ 0 = R_r \cdot i_\alpha^r + L_m \cdot \dfrac{di_\alpha^s}{dt} + L_r \cdot \dfrac{di_\alpha^r}{dt} + \omega_r \cdot L_m \cdot i_\beta^s + \omega_r \cdot L_r \cdot i_\beta^r \\ 0 = R_r \cdot i_\beta^r + L_m \cdot \dfrac{di_\beta^s}{dt} + L_r \cdot \dfrac{di_\beta^r}{dt} - \omega_r \cdot L_m \cdot i_\alpha^s - \omega_r \cdot L_r \cdot i_\alpha^r \end{cases} \quad (1)$$

where (v_α^s, v_β^s), (i_α^s, i_β^s), and (i_α^r, i_β^r) are the (αβ) components of the stator voltages, stator currents, and rotor currents, respectively; R_s and R_r stand for the stator- and rotor-resistances, respectively; L_s, L_r, and L_m stand for the stator-, rotor-, and magnetizing- inductances, respectively. Finally, ω_r is the rotor electric speed computed as pole pairs p times the mechanical one.

When the stator winding is disconnected from the supply, the stator currents are set to zero with a dynamic for now assumed ideal for simplifying the analysis but better analyzed in the following sections. Therefore, the equation system ruling the machine becomes:

$$\begin{cases} v_\alpha^s = e_\alpha^s = L_m \cdot \dfrac{di_\alpha^r}{dt} \\ v_\beta^s = e_\beta^s = L_m \cdot \dfrac{di_\beta^r}{dt} \\ 0 = R_r \cdot i_\alpha^r + L_r \cdot \dfrac{di_\alpha^r}{dt} + \omega_r \cdot L_r \cdot i_\beta^r \\ 0 = R_r \cdot i_\beta^r + L_r \cdot \dfrac{di_\beta^r}{dt} - \omega_r \cdot L_r \cdot i_\alpha^r \end{cases} \quad (2)$$

After the stator is disconnected from the supply, it is noted how the stator voltages correspond to the back-emf components (e_α^s, e_β^s) induced by the rotor currents, whose space-state equation system is computed as:

$$\begin{cases} \dfrac{di_\alpha^r}{dt} = -\dfrac{1}{\tau_r} \cdot i_\alpha^r - \omega_r \cdot L_r \cdot i_\beta^r \\ \dfrac{di_\beta^r}{dt} = -\dfrac{1}{\tau_r} \cdot i_\beta^r + \omega_r \cdot L_r \cdot i_\alpha^r \end{cases} \quad (3)$$

where τ_r is the rotor time constant computed as:

$$\tau_r = L_r / R_r \quad (4)$$

After performing some mathematical manipulations, the solutions of (3) are computed as in (5).

$$\begin{cases} i_\alpha^r = I_0^r \cdot e^{-\frac{t}{\tau_r}} \cdot \cos\left(\omega_r \cdot t - \vartheta_0^r\right) \\ i_\beta^r = I_0^r \cdot e^{-\frac{t}{\tau_r}} \cdot \sin\left(\omega_r \cdot t - \vartheta_0^r\right) \end{cases} \quad (5)$$

In (5), ϑ_0^r is the position of the rotor current vector at the time instant in which the stator is disconnected from the supply (t = 0). Since the rotor flux linkage cannot change discontinuously immediately after the stator shut-off, the amplitude of the rotor currents corresponds as follows:

$$I_0^r = \Lambda_0^r / L_r \quad (6)$$

where Λ_0^r is thus the value of the rotor flux linkage before and immediately after the stator shut-off. According to the *dq* model of the machine [16], this value only depends on the *d*-axis stator current injected in the motor immediately before the stator shut-off. However, the *d*-axis current practically corresponds to the no-load current of the motor for the considered supply voltage level. In other words, the load condition of the motor before the stator shut-off does not affect the flux decay transient.

By replacing (5), (6) in (2), the stator voltages, i.e., the machine's back-emf components, are thus computed as:

$$\begin{cases} v_\alpha^s = e_\alpha^s = e_s \cdot \cos\left(\omega_r \cdot t - \vartheta_0^s\right) \\ v_\beta^s = e_\beta^s = e_s \cdot \sin\left(\omega_r \cdot t - \vartheta_0^s\right) \end{cases} \quad (7)$$

where ϑ_0^s is the position of the back-emf vector at the stator shut-off. Conversely, e_s is the amplitude of the machine's back-emf computed as:

$$e_s = \frac{L_m}{L_r} \cdot \Lambda_0^r \cdot \sqrt{\frac{1}{\tau_r^2} + \omega_r^2} \cdot e^{-\frac{t}{\tau_r}} \quad (8)$$

After applying the inverse Clarke transformation [T], the stator voltages are thus computed in phase coordinates as:

$$v_{123}^s = \left[T_C\right]^{-1} \cdot v_{\alpha\beta}^s = e_s \cdot \begin{bmatrix} \cos\left(\omega_r \cdot t - \vartheta_0^s\right) \\ \cos\left(\omega_r \cdot t - \vartheta_0^s - \frac{2\pi}{3}\right) \\ \cos\left(\omega_r \cdot t - \vartheta_0^s - \frac{4\pi}{3}\right) \end{bmatrix} \quad (9)$$

According to (9), the time constant associated with the decay of the machine's back-emf corresponds to the rotor time constant since the variations of the rotor speed are negligible while the decay transient happens. Hence, justifying the name "flux-decay test" and allowing its execution to evaluate the rotor time constant. However, although the solutions above have been computed assuming the linearity of the equation system ruling the rotor currents (3), the following nonlinearities must be considered.

- The magnetizing inductance L_m is not constant due to the saturation phenomena involving both the stator and rotor laminations [18], [19].
- The rotor leakage inductance L_{lr}, from which the rotor one depends as $L_r = L_m + L_{lr}$, is subjected to saturation phenomena of the rotor leakage fluxes if the rotor slots are closed [19] (see Fig. 2, where some examples of closed rotor slots are reported). Since the die-cast processes for manufacturing the rotor cages lead to closed rotor slots [20], it follows that the saturation phenomena involving the rotor leakage inductance are often present. In addition, it is highlighted how also the skin effect affects the value of L_{lr}.
- The rotor resistance R_r depends on the rotor temperature and is also affected by skin effect phenomena [18], [19].

For these reasons, the rotor time constant is not a constant parameter as it depends on the electromagnetic and thermal conditions of the machine. The primary source of variation consists of the skin effect. It is particularly significant when the rotor time constant is computed by measuring the rotor resistance and rotor leakage inductance with a standard locked-rotor test. In this case, the rotor currents have the same frequency as the stator ones, thus maximizing the impact of the skin effect. Therefore, performing the flux-decay test allows getting the following advantages.

- The rotor time constant can be measured at the rated flux linkage conditions, thus including the saturation of the jumpers when the rotor slots are of a closed shape.
- Magnetic saturation phenomena involving the stator and rotor laminations are included.
- The evaluation of the rotor time constant is not affected by the skin effect on the rotor slots, as it alters the values of both rotor resistance and rotor leakage inductance.
- The flux-decay test can be performed at the rated machine temperature to obtain the rotor time constant at rated operating conditions.

III. Reference Flux-Decay Test

A test has been performed on a 15 kW induction machine to discuss and analyze the flux-decay transient phenomena. The motor characteristics are reported in Appendix. The results of this test will be used as a reference in this paper.

The measurement setup consists of the GEN2tB from HBM Gmbh, i.e., a high-performance data recorder and calibrated data acquisition system. Thanks to its high-voltage/high-speed acquisition channels (voltage card GN610B, 18 bit, 2 MS/s), GEN2tB allows the calibrated measurement of high voltage signals even under pulse-width modulation supply conditions.

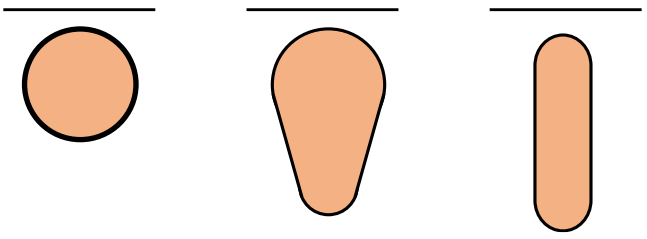


Fig. 2. Examples of closed rotor slots.

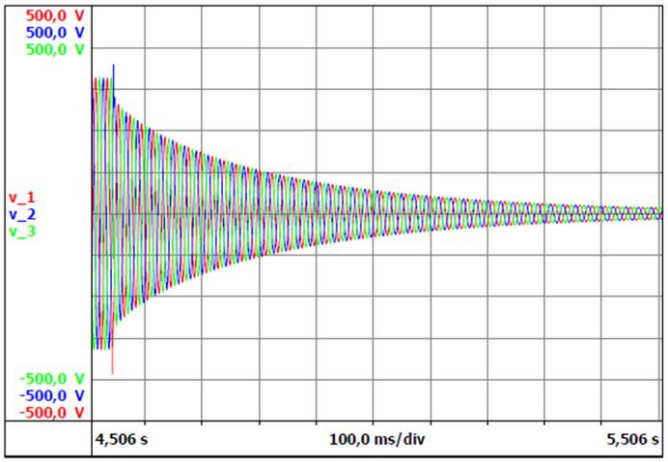


Fig. 3. Measured three-phase stator voltages at the machine terminals.

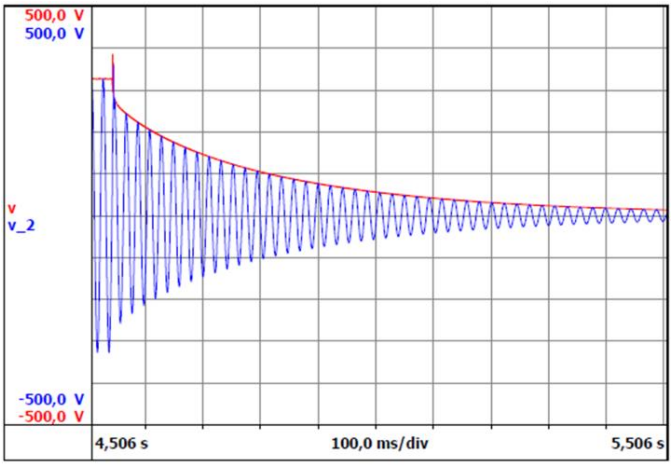


Fig. 4. Envelope of the back-emf decay: voltage of phase *2* (blue) and back-emf amplitude (red).

The flux-decay test was executed at rated voltage, and the measured stator voltages after the stator supply is disconnected are shown in Fig. 3. From this test, the decay of the stator back-emf caused by the decay of the machine rotor flux is well evident. The decay of the back-emf can be analyzed better by plotting the amplitude of the stator voltage vector, as shown in Fig. 4. This plot has been simply obtained by applying the Clarke transformation to the recorded samples of the stator voltages, leading to the computation of the machine's back-emf in stationary (αβ) coordinates as in (10).

$$v^s_{\alpha\beta} = \left[T_C\right] \cdot v^s_{123} \tag{10}$$

The amplitude of the machine's back-emf is thus computed as:

$$e_s = \sqrt{v_\alpha^{s\,2} + v_\beta^{s2}} \tag{11}$$

Starting from the results of the flux-decay test, the amplitude of the machine's back-emf can be fitted using a first-order exponential function *Y* as:

$$Y = X_0 \cdot e^{-t/\tau} \tag{12}$$

where X_0 is the initial value of the considered waveform, while τ is the time constant of the exponential function.

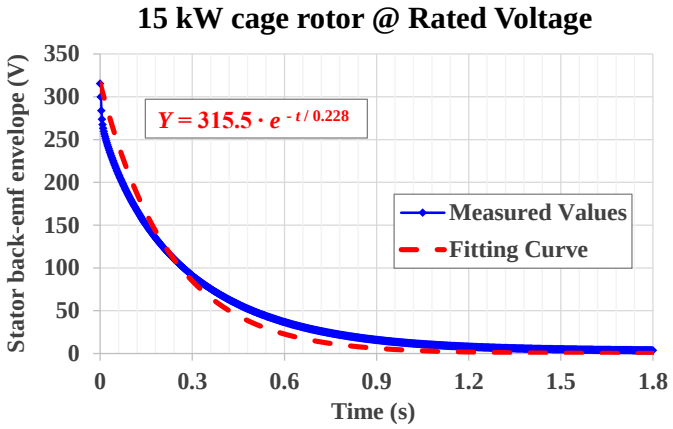


Fig. 5. Measured envelope of the back-emf and fitting curve.

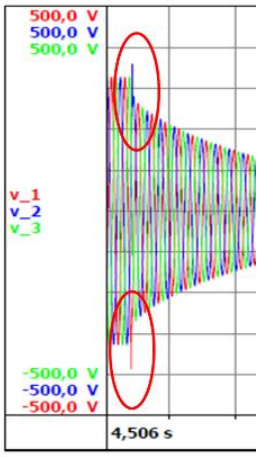


Fig. 6. Stator voltage spikes at the machine terminals.

The measured samples immediately after the stator shut-off directly obtain the initial condition X_0. Then, a conventional spreadsheet can be used to compute the time constant of the exponential by minimizing the sum of the squares of the errors between the fitting exponential (12) and the experimental amplitude waveform. For the motor under test, this leads to the results shown in Fig. 5. It can be seen that the initial point is equal to the peak value of the rated voltage, while the computed rotor time constant τ_r is equal to 228 ms.

According to the theory of the induction machine presented in Section II, the flux-decay is defined by a first-order time-differential equation, thus leading to a single time constant.

However, from the measured back-emf decay, it is well evident that there is an error between the measured amplitude and the fitting curve. This means that the rotor time constant cannot be considered constant during the flux-decay transient. In the following section, this discrepancy will be analyzed. In detail, the flux decay transient will be explained, describing how it is related to the physical phenomena that can influence the value of the rotor time constant.

IV. Physical Phenomena Involved in the Flux-Decay Transient

It follows the description of the phenomena involved during the flux-decay transient.

A. Stator voltage spikes

Even though the voltage spikes have not been included in the data used for the time constant determination (see Fig. 3), it is important to analyze their origin. When the machine is connected to the voltage supply, stator currents are injected. Consequently, the stator leakage inductance is charged with magnetic energy. This energy has to go to zero when the switch is opened. As well known, the stator leakage inductances take into account the leakage fluxes of the stator. These fluxes are not magnetically coupled with the rotor. Therefore, when the stator current is interrupted, the rotor currents cannot support these fluxes. Consequently, the magnetic energy stored in the stator leakage inductance must be dissipated in heat and light produced by the voltage spikes, these last shown in Fig. 6. The stator voltage spikes are therefore unavoidable and are always present during the flux-decay test.

B. Rotor leakage inductance

Looking at Fig. 7, it is well evident that in the early instants of the transient, the back-emf has a sharp reduction, put in evidence by the red circle. Therefore, the initial transient is completely separated from the subsequent one, represented by the first-order differential time-equation (12) instead. This behavior can be justified by looking at the involved physical phenomena. In detail, the reasons are found in the rotor leakage inductance L_{lr}.

The rotor current is very small when the motor operates at no-load conditions because the requested torque is due to friction and ventilation losses. In other words, the rotor can be considered at synchronous speed with a slip close to zero. Consequently, the rotor leakage inductances are uncharged. However, when the switch is opened, the rotor currents have to guarantee the continuity of the rotor flux linkage. Therefore, the rotor leakage inductances must be charged by absorbing energy from the main flux, leading to the subsequent reduction of the back-emf amplitude shown in Fig. 7.

Since the first instants of the back-emf transient are decoupled from the subsequent ones, they should be neglected in determining the rotor time constant. Therefore, Fig. 8 shows the back-emf transient after ignoring the initial measurement data, leading to a computed rotor time constant of 263 ms instead of the previous value of 228 ms. Consequently, it is evident how using the first measured data significantly influences the value of the calculated rotor time constant.

C. Magnetic saturation and iron losses

Even though Fig. 8 shows a good agreement between the measured value and the fitting curve, it is evident that the initial transient shows a different trend from the final one. These two parts can be separately fitted, as shown in Fig. 9 and Fig. 10, where the initial and the final transients are reported. The corresponding rotor time constants are 250 ms and 330 ms, respectively. This analysis shows that there is not a single time constant during the back-emf transient. Indeed, the time constant changes according to the machine flux. The reason can be found in the saturation of the stator and rotor laminations. Equation (4) defines the rotor time constant where the parameters L_r and R_r are variable for different reasons.

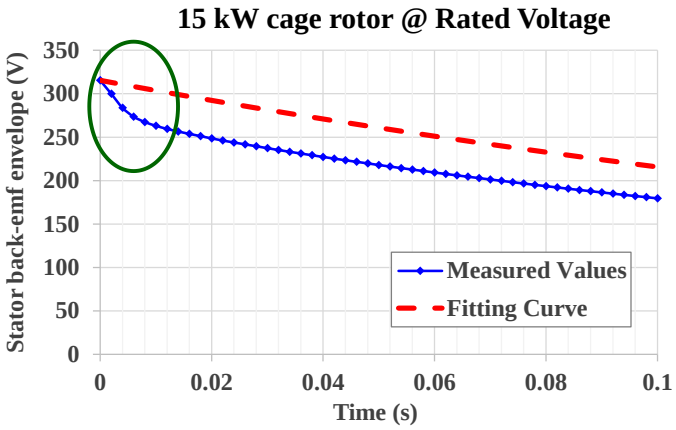


Fig. 7. Magnification of the first instants of the flux-decay test.

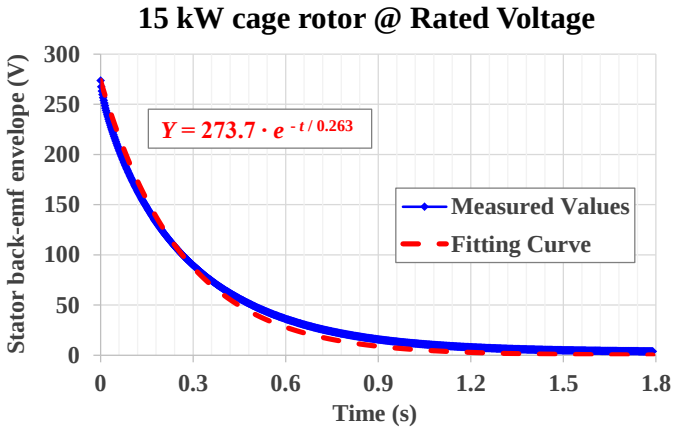


Fig. 8. Back-emf transient by neglecting the initial measurement data.

The rotor resistance R_r depends on the rotor cage temperature, which is constant during the flux decay test. Also, R_r depends on the skin effect of the squirrel cage rotor. However, the rotor currents are unidirectional during the flux decay transient, as measured and discussed in [14]. As a consequence, the skin effect is negligible in the rotor slots.

Nevertheless, it is important to point out that R_r does not represent only the rotor cage resistance and related Joule losses because the stator iron losses are present during the flux decay test. Because the rotor Joule losses depend on the rotor current, to consider the stator iron losses, an additional resistance R_{ir} must be added in series to R_r, defining an equivalent rotor resistance $R_{r,eq}$ as:

$$R_{r,eq} = R_r + R_{ir} \tag{13}$$

Therefore, the definition of the rotor time constant $\tau_{r,eq}$ can be modified as:

$$\tau_{r,eq} = \frac{L_m + L_{lr}}{R_r + R_{ir}} \tag{14}$$

According to (14), the following considerations can be made:

- The magnetizing inductance L_m is affected by magnetic saturation because of the variable permeability of the

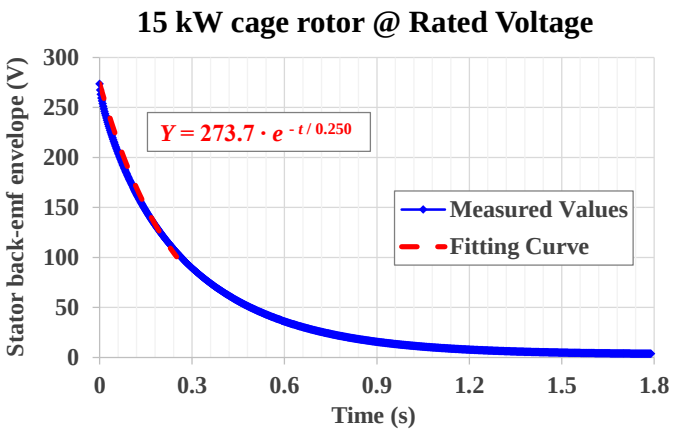


Fig. 9. Back-emf transient at the beginning of the flux-decay test.

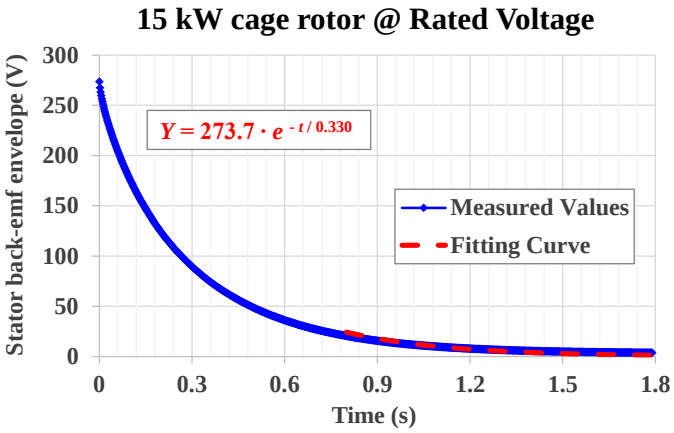


Fig. 10. Back-emf transient at the end of the flux-decay test.

laminations. Consequently, during the flux-decay transient, the magnetizing inductance changes according to the saturation conditions of the laminations.

- The rotor leakage inductance L_{lr} is affected by skin effect phenomena like the rotor resistance, especially if considering squirrel-cage induction machines. However, as previously discussed, the skin effect can be neglected during the flux decay test. On the other hand, since the rotor slots are closed in squirrel cage rotors, the bridges closing the rotor slots are affected by saturation due to the rotor currents [19], making the rotor leakage inductance not constant. In any case, it is highlighted how the magnetizing inductance is much higher than the leakage one, regardless of the saturation conditions. Therefore, according to (14), the rotor time constant is mainly affected by the variations of the magnetizing inductance.

TABLE I summarizes the obtained rotor time constant values. It is noted how the obtained values of the rotor time constants confirm the previous considerations. In fact, with the reduction of the back-emf, i.e., the machine flux, the lamination goes out from the saturation, thus increasing the magnetizing inductance with subsequent reduction of the equivalent rotor resistance in (13).

TABLE I. ROTOR TIME CONSTANT VARIATION

Transient interval	Rotor time constant τ_r (ms)
Initial	250
Total	263
Final	330

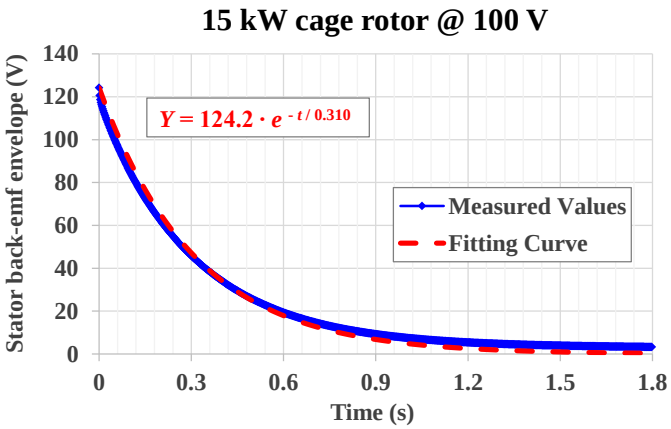


Fig. 11. Flux-decay results for a supply voltage of 100 V.

A flux-decay test at a reduced voltage of 100 V has been performed to confirm the previous results further. Fig. 11 shows the obtained results, where a rotor time constant equal to 310 ms has been computed, thus very close to the one obtained in the final transient (see TABLE I) at the rated voltage (see Fig. 10 from 0.8 s onward).

From a practical point of view, the rotor time constant obtained at rated supply conditions without including the time instants immediately after the stator shut-off represents the best compromise among the many values that this parameter can assume. Therefore, it is recommended to use this value when the torque control of the motor is performed by implementing FOC algorithms, as demonstrated in [16].

D. Additional considerations

From the accuracy point of view, the flux-decay test allows a more accurate determination if considering getting the rotor time constant from the typical no-load and locked-rotor tests. Indeed, the values of rotor resistance and rotor leakage inductance obtained from the results of the locked-rotor test are significantly affected by the skin effect. This consideration is justified by the fact that the locked-rotor test is performed at a given stator frequency f_s that does not correspond to the operative frequency of the rotor f_r since this depends on the slip s as follows:

$$f_r = s \cdot f_s \tag{15}$$

Since the slip is very small in the effective machine's operative condition (a few percent), the rotor frequency is also small, with a negligible impact caused by the skin effect.

The motor has been tested in locked-rotor conditions in the frequency range of 2 Hz – 50 Hz to confirm the previous considerations. In addition, the no-load test has been performed to determine the magnetizing inductance L_m.

TABLE II. NO-LOAD AND LOCKED ROTOR TEST RESULTS AT VARIOUS SUPPLY FREQUENCIES

Frequency (Hz)	L_m (H)	L_{lr} (H)	R_r (Ω)
50	0.0351	0.00254	0.557
40	0.0351	0.00267	0.488
30	0.0351	0.00284	0.401
20	0.0351	0.00307	0.302
10	0.0351	0.00337	0.214
5	0.0351	0.00372	0.176
2	0.0351	0.00533	0.151
0 (extrapolation)	0.0351	0.00680	0.132

TABLE III. ROTOR TIME CONSTANT VALUES OBTAINED FROM THE NO-LOAD AND LOCKED ROTOR TESTS

Frequency (Hz)	Rotor time constant τ_r (ms)	Error (%)
50	67.6	-62.3
40	77.4	-59.2
30	94.6	-53.7
20	126.4	-43.6
10	179.8	-26.6
5	220.6	-13.5
2	267.7	+1.5
0 (extrapolation)	316.5	+16.9
Flux decay test	**263.0**	-

TABLE II summarizes the obtained results. TABLE III instead compares the rotor time constants computed using the results of the no-load and locked-rotor tests with the value of the rotor time constant obtained by performing the flux-decay test. Since the magnetizing inductance does not depend on the rotor frequency, its value has been considered constant.

Fig. 12 shows the trend of the rotor time constant evaluated using the no-load and the locked-rotor tests as a function of the supply frequency, i.e., the rotor frequency according to (15) since $s = 1$ in locked-rotor conditions. As expected, the rotor time constant value computed at the rated stator frequency of 50 Hz is wrong from the value obtained using the flux decay test. The error is higher than 60 %, confirming the influence of the skin effect on the rotor time constant. Conversely, the skin effect is not active when the motor is working in its operative conditions, i.e., when the rotor frequency is a few Hz. In particular, for the motor under test, the rated slip is equal to 0.04, corresponding to a rotor frequency of 2 Hz.

Therefore, considering the results of the locked-rotor test at the rated slip frequency of 2 Hz (see TABLE II), i.e., a rotor resistance of 151 mΩ and a rotor leakage inductance of 5.33 mH, the computed rotor time constant is 267.7 ms. Since the rotor time constant computed when performing the flux decay test is 263 ms, the two values can be considered coincident (see Fig. 12). This result confirms the validity of the flux decay test, which can be considered the best approach for determining the rotor time constant to other approaches, particularly those based on the no-load and the locked rotor tests.

Finally, it is noted how TABLE II and TABLE III also report the extrapolated values of rotor resistance $R_{r,0}$ and rotor leakage inductance $L_{lr,0}$ for a null rotor frequency, obtained according to the experimental profiles shown in Fig. 13 and Fig. 14.

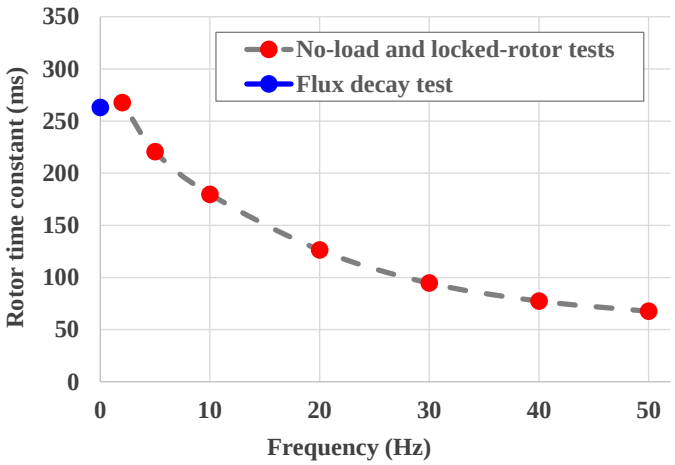


Fig. 12. Rotor time constant as a function of the frequency and comparison with the value obtained with the flux decay test.

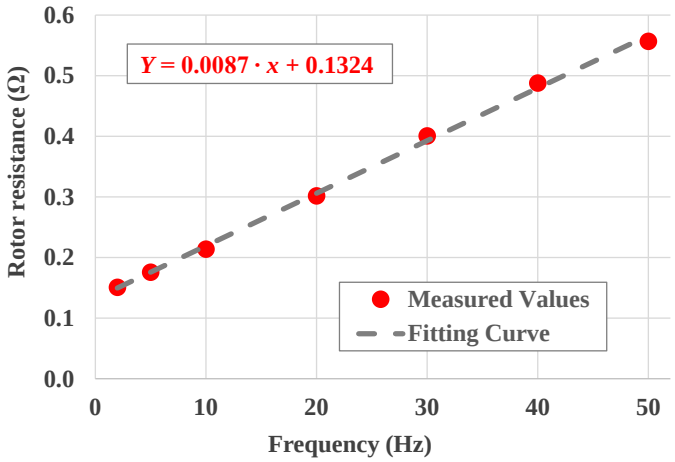


Fig. 13. Rotor resistance as a function of the frequency.

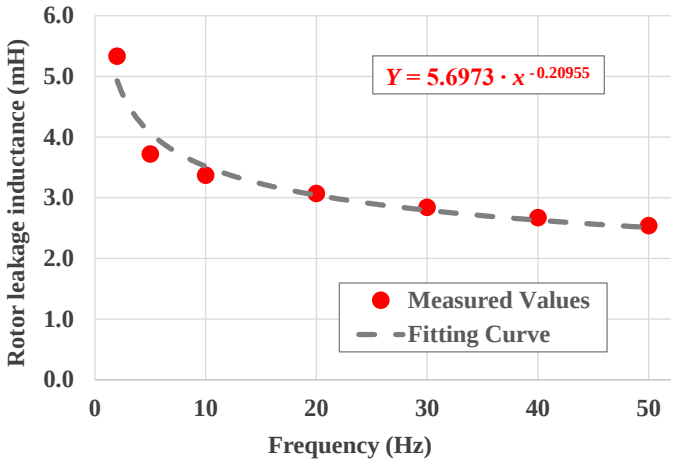


Fig. 14. Rotor leakage inductance as a function of the frequency.

This way, the equivalent rotor resistance $R_{r,eq}$ considering the iron losses contribution R_{ir} can be estimated as:

$$R_{ir} = R_{r,eq} - R_{r,0} = \frac{L_m + L_{lr,0}}{\tau_{r,eq}} - R_{r,0} \tag{16}$$

By applying (16) and considering the rotor time constant values reported in TABLE I, the results reported in TABLE IV are obtained.

TABLE IV. ADDITIONAL ROTOR RESISTANCE DUE TO THE IRON LOSSES

Transient interval	τ_r (ms)	$R_{r,eq}$ (mΩ)	R_{ir} (mΩ)
Initial	250	167.6	35.2
Total	263	159.3	26.9
Final	330	127.0	-5.4

It is noted how the results in TABLE IV confirm the previously reported considerations about iron losses (see subsection IV-C). Indeed, during the initial transient of the flux decay test, the iron losses significantly impact the actual rotor time constant, leading to an additional resistance of R_{ir} = 35.2 mΩ, a value of about 21 % of the overall equivalent rotor resistance $R_{r,eq}$ = 167.6 mΩ. Conversely, considering the final transient of the flux decay test, the additional resistance is effectively insignificant due to the absence of iron losses.

V. CONCLUSION

In this paper, a detailed analysis of the physical phenomena involved during the flux-decay test has been reported. Experimental results obtained on a squirrel-cage induction motor rated 15 kW have shown that the rotor time constant significantly changes during the flux-decay transient due to several electromagnetic phenomena like magnetic saturation of the machine's lamination and stator iron losses. Therefore, this paper has provided the guidelines to correctly elaborate the results of the flux decay test, allowing an accurate evaluation of the rotor time constant. Moreover, a comparison between the rotor time constant value obtained from the proposed analysis with that obtained from the elaboration of the conventional no-load and locked rotor tests has been performed. According to the experimental results, the rotor time constant obtained by performing the flux decay test can be considered the most accurate value because it represents the actual working condition of the machine. In contrast, the results obtained from the locked-rotor test are strictly affected by the skin effect phenomenon, making it necessary to perform this test at a supply frequency near the rated slip frequency of the motor. In addition, it is highlighted that the execution of the flux decay test allows obtaining a rotor time constant value corresponding to the actual rotor temperature. Thus, without needing any manipulation toward the temperature-rescaling, as for the no-load and locked-rotor test results.

In conclusion, the contributions of this paper to the existing literature are summarized as follows.

1) Provide a detailed analysis of the electromagnetic phenomena involved during the flux decay test.
2) Provide the guidelines for correctly elaborating the flux decay test results. Hence, obtaining an accurate value of the rotor time constant to be used for the implementation of torque control algorithms of the machine.

APPENDIX

TABLE V lists the rated data of the motor used for the experimental tests, whose view is shown in Fig. 15. The rotor slots of the machine are shown in Fig. 16, where it is noted how they are closed with an "umbrella" shape.

TABLE V. RATED DATA OF THE MOTOR UNDER TEST

Rated Power	15 kW
Number of Poles	4
Rated Speed	1440 r/m
Rated Voltage	380 V
Rated Current	32.5 A
Rated Frequency	50 Hz



Fig. 15. View of the motor under test.

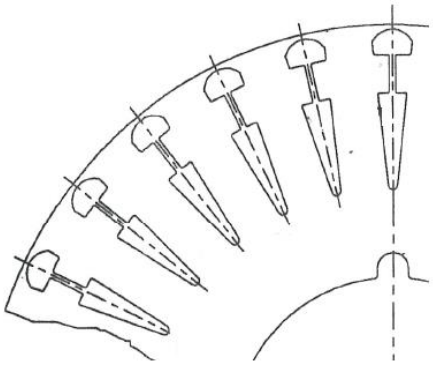


Fig. 16. Section or the rotor slots of the motor under test.

VI. REFERENCES

[1] S.-H. Kim, *Electric Motor Control: DC, AC and BLDC Motors*. Elsevier, 2017.

[2] I. Ferdiansyah, M. R. Rusli, B. Praharsena, H. Toar, Ridwan, and E. Purwanto, 'Speed Control of Three Phase Induction Motor Using Indirect Field Oriented Control Based on Real-Time Control System', in *2018 10th International Conference on Information Technology and Electrical Engineering (ICITEE)*, Jul. 2018, pp. 438–442. doi: 10.1109/ICITEED.2018.8534864.

[3] Bin Lu, T. G. Habetler, and R. G. Harley, 'A survey of efficiency-estimation methods for in-service induction motors', *IEEE Trans. Ind. Appl.*, vol. 42, no. 4, pp. 924–933, Jul. 2006, doi: 10.1109/TIA.2006.876065.

[4] S. Chacko, C. Bhende, S. Jain, and R. Nema, 'Modeling and Simulation of Field Oriented Control Induction Motor Drive and Influence of Rotor Resistance Variations on its Performance', *Electr. Electron. Eng. Int. J.*, vol. 5, no. 1, Feb. 2016, doi: 10.14810/elelij.2016.5103.

[5] C. Wang, D. W. Novotny, and T. A. Lipo, 'An automated rotor time-constant measurement system for indirect field-oriented drives', *IEEE Trans. Ind. Appl.*, vol. 24, no. 1, pp. 151–159, Jan. 1988, doi: 10.1109/28.87266.

[6] W. H. Kwon, C. H. Lee, K. S. Youn, and G. H. Cho, 'Measurement of rotor time constant taking into account magnetizing flux in the induction motor', in *Proceedings of 1994 IEEE Industry Applications Society Annual Meeting*, Oct. 1994, vol. 1, pp. 88–92 vol.1. doi: 10.1109/IAS.1994.345494.

[7] S. Wade, W. Dunnigan, and B. W. Williams, 'A new method of rotor resistance estimation for vector-controlled induction machines', *IEEE Trans. Ind. Electron.*, vol. 44, no. 2, pp. 247–257, Apr. 1997, doi: 10.1109/41.564164.
[8] J. Laowanitwattana and S. Uatrongjit, 'Estimation of induction motor states and parameters based on Extended Kalman Filter considering parameter constraints', in *2016 International Symposium on Power Electronics, Electrical Drives, Automation and Motion (SPEEDAM)*, Jun. 2016, pp. 755–760. doi: 10.1109/SPEEDAM.2016.7525829.
[9] Li-Cheng Zai, C. L. DeMarco, and T. A. Lipo, 'An extended Kalman filter approach to rotor time constant measurement in PWM induction motor drives', *IEEE Trans. Ind. Appl.*, vol. 28, no. 1, pp. 96–104, Jan. 1992, doi: 10.1109/28.120217.
[10] E. Bim, 'Fuzzy optimization for rotor constant identification of an indirect FOC induction motor drive', *IEEE Trans. Ind. Electron.*, vol. 48, no. 6, pp. 1293–1295, Dec. 2001, doi: 10.1109/41.969416.
[11] S. Yang, D. Ding, X. Li, Z. Xie, X. Zhang, and L. Chang, 'A Novel Online Parameter Estimation Method for Indirect Field Oriented Induction Motor Drives', *IEEE Trans. Energy Convers.*, vol. 32, no. 4, pp. 1562–1573, Dec. 2017, doi: 10.1109/TEC.2017.2699681.
[12] A. N. Smith, S. M. Gadoue, and J. W. Finch, 'Improved Rotor Flux Estimation at Low Speeds for Torque MRAS-Based Sensorless Induction Motor Drives', *IEEE Trans. Energy Convers.*, vol. 31, no. 1, pp. 270–282, Mar. 2016, doi: 10.1109/TEC.2015.2480961.
[13] B. Karanayil, M. F. Rahman, and C. Grantham, 'Rotor resistance identification using artificial neural networks for a speed sensorless vector controlled induction motor drive', in *IECON'03. 29th Annual Conference of the IEEE Industrial Electronics Society (IEEE Cat. No.03CH37468)*, Nov. 2003, vol. 1, pp. 419–424 vol.1. doi: 10.1109/IECON.2003.1280017.
[14] E. Armando, A. Boglietti, S. Musumeci, and S. Rubino, 'Induction Motor Rotor Time-Constant Determination using Flux-Decay Test', in *2020 International Conference on Electrical Machines (ICEM)*, Aug. 2020, vol. 1, pp. 1164–1170. doi: 10.1109/ICEM49940.2020.9270928.
[15] E. Armando, A. Boglietti, F. Mandrile, E. Carpaneto, and S. Rubino, 'A Detailed Analysis of the Electromagnetic Phenomena Observed During the Flux-Decay Test', in *2022 International Conference on Electrical Machines (ICEM)*, Sep. 2022, pp. 767–773. doi: 10.1109/ICEM51905.2022.9910822.
[16] E. Armando, A. Boglietti, F. Mandrile, and S. Rubino, 'Torque Control Accuracy Using Different Techniques for Determination of Induction Motor Rotor Time Constant', in *2022 International Conference on Electrical Machines (ICEM)*, Sep. 2022, pp. 572–578. doi: 10.1109/ICEM51905.2022.9910671.
[17] P. Krause, O. Wasynczuk, S. D. Sudhoff, and S. Pekarek, *Analysis of Electric Machinery and Drive Systems*. John Wiley & Sons, 2013.
[18] A. Boglietti, A. Cavagnino, and M. Lazzari, 'Computational Algorithms for Induction-Motor Equivalent Circuit Parameter Determination—Part I: Resistances and Leakage Reactances', *IEEE Trans. Ind. Electron.*, vol. 58, no. 9, pp. 3723–3733, Sep. 2011, doi: 10.1109/TIE.2010.2084974.
[19] A. Boglietti, A. Cavagnino, and M. Lazzari, 'Computational Algorithms for Induction Motor Equivalent Circuit Parameter Determination—Part II: Skin Effect and Magnetizing Characteristics', *IEEE Trans. Ind. Electron.*, vol. 58, no. 9, pp. 3734–3740, Sep. 2011, doi: 10.1109/TIE.2010.2084975.
[20] A. Boglietti, R. I. Bojoi, A. Cavagnino, P. Guglielmi, and A. Miotto, 'Analysis and Modeling of Rotor Slot Enclosure Effects in High-Speed Induction Motors', *IEEE Trans. Ind. Appl.*, vol. 48, no. 4, pp. 1279–1287, Jul. 2012, doi: 10.1109/TIA.2012.2199270.

VII. BIOGRAPHIES



Eric Armando (M'15, SM'19) received the M.Sc. and Ph.D. degrees in Electrical Engineering from Politecnico di Torino, Turin, Italy, in 2002 and 2008, respectively. He is now with Politecnico di Torino as a Full Professor of Power Converters, Electrical Machines, and Drives. His fields of interest are power electronics and high-performance ac motor drives. Prof. Armando is co-author of numerous Journal Papers and three Patents. Over the years, he received three awards for innovation and one paper award from the Power Electronics Technical Committee of the IEEE Industrial Electronics Society.



Aldo Boglietti (M'04, SM'06, F'12) was born in Rome, Italy in 1957. He received the Laurea degree in Electrical Engineering from Politecnico di Torino, Italy, in 1981. He started his research work with the Department of Electrical Engineering of the Politecnico di Torino as a researcher in Electrical Machines in 1984. He was Associate Professor in Electrical Machines in 1992, and now he is a Full Professor at the same University since November 2000. He was head of the Electrical Engineering Department of the Politecnico of Torino from 2003 until 2011. He is an IEEE Fellow Member and Past Chair of the Electrical Machine Committee of IEEE Industry Application Society and Past Chair of the Electrical Machine Technical Committee of IEEE Industrial Electronics Society. In 2020 He got the ICEM International Conference on Electrical Machine Arthur Ellison Outstanding Achievement Award. Aldo Boglietti is the author of more than 150 papers in the field of energetic problems in electrical machines and drives, high-efficiency industrial motor, magnetic material and their applications in electrical machines, electrical machines, and drives models, thermal problems in electrical machines.



Fabio Mandrile (S'18, M'21) received the M.Sc. and Ph.D. degrees in electrical engineering in 2017 and 2021, respectively, from Politecnico di Torino, Torino, Italy. His main research interests include virtual synchronous generators, power electronics for grid-connected applications, and the experimental characterization of converters and motor drives.



Enrico Carpaneto (M'86) was born in Torino, Italy, in 1959. He received the M.Sc. and Ph.D. degrees in electrical engineering from Politecnico di Torino, Torino, Italy, in 1984 and 1989, respectively. He is currently an Associate with the Energy Department, Politecnico di Torino. His research activities cover many different aspects of modeling, simulation, and optimization of generation, transmission and distribution systems. He has published more than 100 scientific papers. He has been responsible for several research contracts concerning analysis, operation, and planning of distribution networks, power quality, and generation optimization. His current research interests include distribution systems, dispersed generation, virtual synchronous generators, and thermal models. Dr. Carpaneto is a member of the IEEE Power Engineering Society and Associazione Italiana di Elettrotecnica, Elettronica, Automazione, Informatica e Telecomunicazioni (AEIT).



Sandro Rubino (S'16, M'18) received the M.Sc. and Ph.D. degrees in Electrical Engineering from Politecnico di Torino, Torino, Italy, in 2014 and 2019, respectively. He is currently Assistant Professor with Dipartimento Energia "G. Ferraris," Politecnico di Torino. He serves as a reviewer for some IEEE Transactions and international conferences. His main research interests include power electronics, modeling, and control of multiphase electrical machines and high-performance ac motor drives. He was the recipient of two paper awards from the Industrial Drives Committee of the IEEE Industry Applications Society and two Ph.D. thesis awards from the IEEE Power & Energy Society Italy Chapter and the IEEE Industrial Electronics Society Italy Chapter, respectively.